EEG Reconstruction with a Dual-scale CNN-LSTM Model for Deep Artifact Removal - Supplementary Materials

Tengfei Gao, Dan Chen*Member, IEEE*, Yunbo Tang, Zhekai Ming, and Xiaoli Li

I. Supplementary Materials

A. Formal Flowchart for DuoCL

A formal flowchart for *DuoCL* is presented in Algorithm 1.

Algorithm 1 Artifacts removal by DuoCL

1: Use sliding window to segment raw EEG ;
2: Normalize the raw EEG segment following the normalization formula:

$$\hat{y} = \frac{y}{\sigma(y)}. \tag{1}$$

3: Construct the network of artifact removal model;
4: Adjust the parameters to minimize the loss during the training process;
5: Normalize the raw EEG to be tested and feed it into the trained model, then multiply the output by the standard deviation of the raw EEG to obtain the artifact-free EEG.

B. Dataset construction pipeline

To quantify the performance of the methods, three semi-simulated datasets were constructed, including two single-channel EEG datasets ((Dataset: I & II)) and one multi-channel EEG dataset (Dataset: III). Contaminated EEG (EEG_C) was simulated by manually contaminating pure EEG (EEG_P) with artifacts and the EEG and artifacts used are all real data. For Dataset: I & II), the semi-simulated contaminated EEG dataset construction pipeline was shown in Fig. 1. Pure EEG segments were generated using the EEG dataset[1] from $GigaDB$. Inspired by [1], the EEG data were processed as follows: First, the data were band-pass filtered between 1 and 80Hz, notched at powerline frequency, then re-sampled to 256Hz. The obtained EEG data were then intercepted using the ICLabel toolbox [2] as the ground truth. Finally, using a sliding window, the pure EEG signal was segmented into a series of one-dimensional segments of length 2s. Artifact data were derived from multiple open-access datasets[2] [3]–[7]. The processing of these artifact data was similar to that of the EEG. For the EMG artifacts, facial EMG data were selected because they were the main sources of EMG artifacts in the EEG. The

[1]Authorized for open access at the website: http://gigadb.org/dataset/100295
[2]Authorized for open access at the website: https://archive.physionet.org

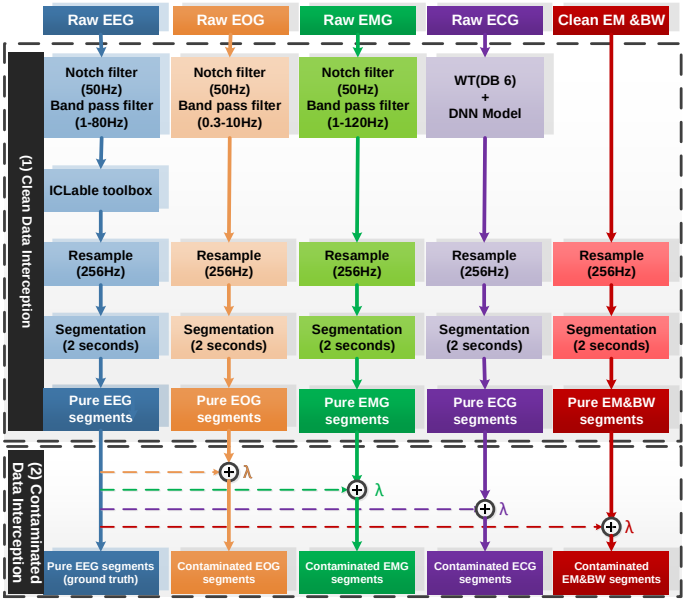

Fig. 1: Pipeline of constructing the semi-simulated contaminated EEG dataset.

frequency range during EMG filtering was set at 1-120 Hz. For EOG artifacts, the horizontal and vertical raw EOG data were band-pass filtered between 0.3 and 10Hz rather than 1 and 80 Hz. For ECG artifacts, the raw ECG data used the method proposed by [8] to obtain pure ECG data. Furthermore, because the two types of acquired non-physiological artifact data acquired were already processed, only resampling and segmentation were used.

To evaluate the performance of the model in removing artifacts from multi-channel EEG, **Dataset III** was constructed using a subset of the public dataset (KLADOS) [9] which was designed for the comparison of EOG artifact removal methods. The EEG data of the KLADOS dataset were collected from 27 healthy adults, 13 females and 14 males, during an eye-closed session. The international 10–20 system was applied to place the 19 electrodes (FP1, FP2, F3, F4, C3, C4, P3, P4, O1, O2, F7, F8, T3, T4, T5, T6, Fz, Cz, Pz). The sampling frequency for these data was 200 Hz and band pass filtered at 0.5–40 Hz and notch filtered at 50 Hz were applied. A total of 54 datasets were obtained from 27 subjects, with each dataset having a duration of 30 s. The following equation was used to generate the simulated contaminated EEG:

$$EEG_{C_{i,j}} = EEG_{P_{i,j}} + \lambda_i HEOG + \lambda_j VEOG, \tag{2}$$

where $EEG_{C_{i,j}}$ represented the EEG signals contaminated by ocular artifacts and $EEG_{P_{i,j}}$ represented the EEG signals without ocular artifacts. HEOG and VEOG were horizontal and vertical EOG records, respectively. The vectors λ_i and λ_j represented the contamination coefficients of HEOG and VEOG, respectively. i and j indicated the subject number and electrode's number, respectively.

C. Supplementary Material for Ablation analysis

This section provided schematic diagrams of the models compared in the ablation analysis experiments. The "LSTM" model was the same as in Section I-D, and details were available in Table III.

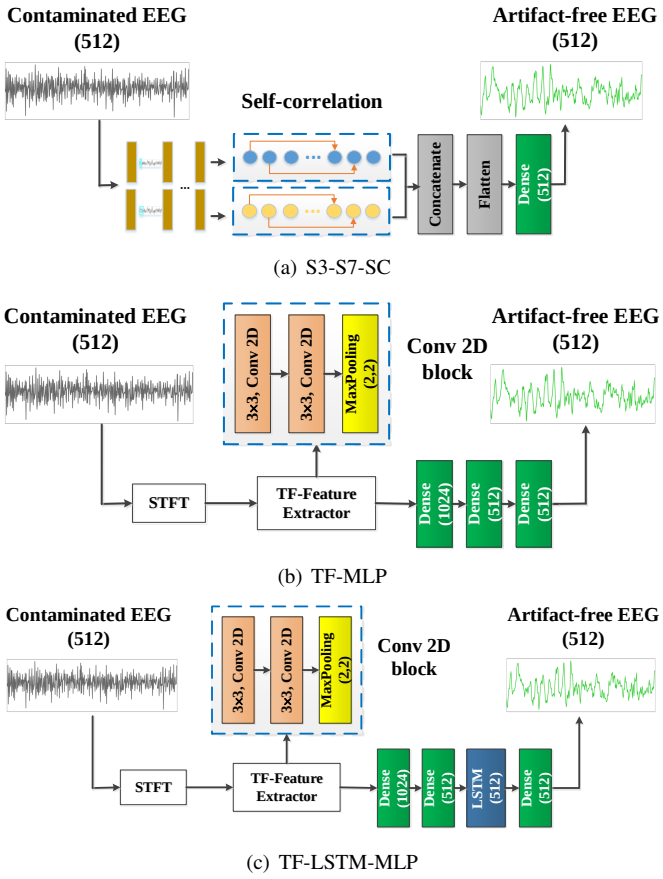

(a) S3-S7-SC

(b) TF-MLP

(c) TF-LSTM-MLP

Fig. 2: Model structures of the methods in ablation analysis

D. Details of the Compared Methods in Performance Experiments

The detailed structures of *DuoCL* and compared DL-based methods were reported in followed five tables (Tables I, II, III, IV, and V) including the network parameters and output of each layer. Two traditional methods: Wiener filtering (WF) and empirical mode decomposition (EMD) were implemented for the performance evaluation. For the WF method, only a portion of the training set with the same artifact type as the data to be processed was used for training filter. For the EMD method, the intrinsic mode functions (IMFs) of artifacts were defined by the distance metric used in hierarchical clustering [10], which was consistent with the literature [1].

TABLE I: Details of DuoCL parameters and network layers

Layer	Kernel unit	Output shape	Connected to
Input	-	(None,512,1)	-
Conv1d-1	1*3,16	(None,512,16)	Input
Conv1d-6	1*7,16	(None,512,16)	Input
Average pooling1d-1	-	(None,256,16)	Conv1d-1
Average pooling1d-5	-	(None,256,16)	Conv1d-6
Conv1d-2	1*3,32	(None,256,32)	Average pooling1d-1
Conv1d-7	1*7,32	(None,256,32)	Average pooling1d-5
Average pooling1d-2	-	(None,128,32)	Conv1d-2
Average pooling1d-6	-	(None,128,32)	Conv1d-7
Conv1d-3	1*3,64	(None,128,64)	Average pooling1d-2
Conv1d-8	1*7,64	(None,128,64)	Average pooling1d-6
Average pooling1d-3	-	(None,64,64)	Conv1d-3
Average pooling1d-7	-	(None,64,64)	Conv1d-8
Conv1d-4	1*3,128	(None,64,128)	Average pooling1d-3
Conv1d-9	1*7,128	(None,64,128)	Average pooling1d-7
Average pooling1d-4	-	(None,32,128)	Conv1d-4
Average pooling1d-8	-	(None,32,128)	Conv1d-9
Conv1d-5	1*3,256	(None,32,256)	Average pooling1d-4
Conv1d-10	1*7,256	(None,32,256)	Average pooling1d-8
Dropout-1	0.2	(None,32,256)	Conv1d-5
Dropout-2	0.2	(None,32,256)	Conv1d-10
Flatten-1	-	(None,8192)	Dropout-1
Flatten-2	-	(None,8192)	Dropout-2
Dense-1	1024	(None,1024)	Flatten-1
Dense-3	1024	(None,1024)	Flatten-2
Dense-2	512	(None,512)	Dense-1
Dense-4	512	(None,512)	Dense-3
LSTM-1	1	(None,512,1)	Dense-2
LSTM-2	1	(None,512,1)	Dense-4
Concatenate-1	axis=-1	(None,512,2)	LSTM-1 & LSTM-2
Flatten-3	-	(None,1024)	Concatenate-1
Dense-5	512	(None,512)	Flatten-3

TABLE II: Detailed parameters used for all layers of FCNN model

Layer	Kernel unit	Output shape	Connected to
Input	-	(None,512,1)	-
Flatten-1	-	(None,512)	Input
Dense-1	512	(None,512)	Flatten-1
Dropout-1	0.3	(None,512)	Dense-1
Dense-2	512	(None,512)	Dropout-1
Dropout-2	0.3	(None,512)	Dense-2
Dense-3	512	(None,512)	Dropout-2
Dropout-3	0.3	(None,512)	Dense-3
Dense-4	512	(None,512)	Dropout-3

E. Results evaluation

To give a more detailed presentation of the result analysis, the waveform results of eliminating EOG, ECG, and EM artifacts from the contaminated EEG at SNR= 0 dB using the seven methods were shown in Fig. 3, 4, and 5, respectively. The black line indicated the raw EEG with artifacts, whereas the red and green lines indicated the pure EEG and reconstructed EEG, respectively.

Figs. 6, 7, 8, and 9 gave the waveform results after removing unknown and mixed artifacts for the comparison methods.

TABLE III: Detailed parameters used for all layers of LSTM model

Layer	Kernel unit	Output shape	Connected to
Input	-	(None,512,1)	-
LSTM	1	(None,512,1)	Input
Flatten-1	-	(None,512)	LSTM
Dense-1	512	(None,512)	Flatten-1
Dropout-1	0.3	(None,512)	Dense-1
Dense-2	512	(None,512)	Dropout-1
Dropout-2	0.3	(None,512)	Dense-2
Dense-3	512	(None,512)	Dropout-2

TABLE IV: Detailed parameters used for all layers of 1D-ResCNN

Layer	Kernel unit	Output shape	Connected to
Input	-	(None,512,1)	-
Conv1d-1	1*5,32	(None,512,32)	Input
BN-1	-	(None,512,32)	Conv1d-1
ResBlock1	(kernel size:1*3)		
Conv1d-2	1*3,32	(None,512,32)	BN-1
BN-2	-	(None,512,32)	Conv1d-2
Conv1d-3	1*3,16	(None,512,16)	BN-2
BN-3	-	(None,512,16)	Conv1d-3
Conv1d-4	1*3,32	(None,512,32)	BN-3
BN-4	-	(None,512,32)	Conv1d-4
Add-1	-	-	BN-1& BN-4
Conv1d-5	1*3,32	(None,512,32)	Add-1
BN-5	-	(None,512,32)	Conv1d-5
Conv1d-6	1*3,16	(None,512,16)	BN-5
BN-6	-	(None,512,16)	Conv1d-6
Conv1d-7	1*3,32	(None,512,32)	BN-6
BN-7	-	(None,512,32)	Conv1d-7
Add-2	-	-	BN-4 & BN-7
ResBlock2	(kernel size:1*5)		
...			
Add-4	-	-	BN-10 & BN-13
ResBlock3	(kernel size:1*7)		
...			
Add-6	-	-	BN-16 & BN-19
Concatenate-1	axis=-1	(None,512,96)	Add-2 & Add-4 & Add-6
Conv1d-20	1*1,32	(None,512,32)	Concatenate-1
BN-20	-	(None,512,32)	Conv1d-20
Flatten-1	-	(None,16384)	BN-20
Dense-1	512	(None,512)	Flatten-3

BN: BatchNormalization
ResBlock1, ResBlock2, and ResBlock3 have the same structure except for the kernel size.

TABLE V: Detailed parameters used for all layers of Novel-CNN

Layer	Kernel unit	Output shape	Connected to
Input	-	(None,512,1)	-
Conv1d-1	1*3,32,1	(None,512,32)	Input
Conv1d-2	1*3,32,1	(None,512,32)	Conv1d-1
Average pooling1d-1	2	(None,256,32)	Conv1d-2
Conv1d-3	1*3,64,1	(None,256,64)	Average pooling1d-1
Conv1d-4	1*3,64,1	(None,256,64)	Conv1d-3
Average pooling1d-2	2	(None,128,64)	Conv1d-4
Conv1d-5	1*3,128,1	(None,128,128)	Average pooling1d-2
Conv1d-6	1*3,128,1	(None,128,128)	Conv1d-5
Average pooling1d-3	2	(None,64,128)	Conv1d-6
Conv1d-7	1*3,256,1	(None,64,256)	Average pooling1d-3
Conv1d-8	1*3,256,1	(None,64,256)	Conv1d-7
Average pooling1d-4	2	(None,32,256)	Conv1d-8
Conv1d-9	1*3,512,1	(None,32,512)	Average pooling1d-4
Conv1d-10	1*3,512,1	(None,32,512)	Conv1d-9
Dropout-1	0.5	(None,32,512)	Conv1d-10
Average pooling1d-5	2	(None,16,512)	Conv1d-10
Conv1d-11	1*3,1024,1	(None,16,1024)	Average pooling1d-5
Conv1d-12	1*3,1024,1	(None,16,1024)	Conv1d-11
Dropout-2	0.5	(None,32,512)	Conv1d-12
Average pooling1d-6	2	(None,8,1024)	Conv1d-12
Conv1d-13	1*3,2048,1	(None,8,2048)	Average pooling1d-6
Conv1d-14	1*3,2048,1	(None,8,2048)	Conv1d-13
Dropout-3	0.5	(None,32,512)	Conv1d-14
Flatten-1	-	(None,16384)	Dropout-14
Dense-1	512	(None,512)	Flatten-1

Fig. 10 provided the results of each method for removing unknown & hybrid artifacts at different SNR levels, and the results indicated that the data quality improved at all levels after artifact removal, with $DuoCL$ performing better.

In addition, the results of the SNR, RRMSE$_f$ and CC before and after the hybrid artifact (EMG+EOG+BW+ECG) removal via *DuoCL* were shown in Fig. 11. All three of them performed consistently with RRMSE$_t$ in their results.

REFERENCES

[1] H. Zhang, M. Zhao, C. Wei, D. Mantini, Z. Li, and Q. Liu, "EEGdenoisenet: A benchmark dataset for deep learning solutions of EEG denoising," *Journal of Neural Engineering*, vol. 18, no. 5, p. 056057, 2021.

[2] L. Pion-Tonachini, K. Kreutz-Delgado, and S. Makeig, "Iclabel: An automated electroencephalographic independent component classifier, dataset, and website," *NeuroImage*, vol. 198, pp. 181–197, 2019.

[8] P. Xiong, H. Wang, M. Liu, S. Zhou, Z. Hou, and X. Liu, "ECG signal enhancement based on improved denoising auto-encoder," *Engineering Applications of Artificial Intelligence*, vol. 52, pp. 194–202, 2016.

[3] A. Schlögl, C. Keinrath, D. Zimmermann, R. Scherer, R. Leeb, and G. Pfurtscheller, "A fully automated correction method of EOG artifacts in EEG recordings," *Clinical Neurophysiology*, vol. 118, no. 1, pp. 98–104, 2007.

[4] M. Fatourechi, A. Bashashati, R. K. Ward, and G. E. Birch, "EMG and EOG artifacts in brain computer interface systems: A survey." *Clinical Neurophysiology*, vol. 118, no. 3, pp. 480–494, 2007.

[5] C. Brunner, M. Naeem, R. Leeb, B. Graimann, and G. Pfurtscheller, "Spatial filtering and selection of optimized components in four class motor imagery EEG data using independent components analysis," *Pattern Recognition Letters*, vol. 28, no. 8, pp. 957–964, 2007.

[6] G. Moody and R. Mark, "The impact of the mit-bih arrhythmia database," *IEEE Engineering in Medicine and Biology Magazine*, vol. 20, no. 3, pp. 45–50, 2001.

[7] G. B. Moody, W. K. Muldrow, and R. G. Mark, "Noise stress test for arrhythmia detectors," *Computers in Cardiology*, vol. 11, pp. 381–384, 1984.

[9] M. A. Klados and P. D. Bamidis, "A semi-simulated EEG/EOG dataset for the comparison of eog artifact rejection techniques," *Data in Brief*, vol. 8, pp. 1004–1006, 2016.

[10] A. Mert and A. Akan, "Hilbert-huang transform based hierarchical clustering for EEG denoising," in *21st European Signal Processing Conference (EUSIPCO 2013)*, 2013, pp. 1–5.

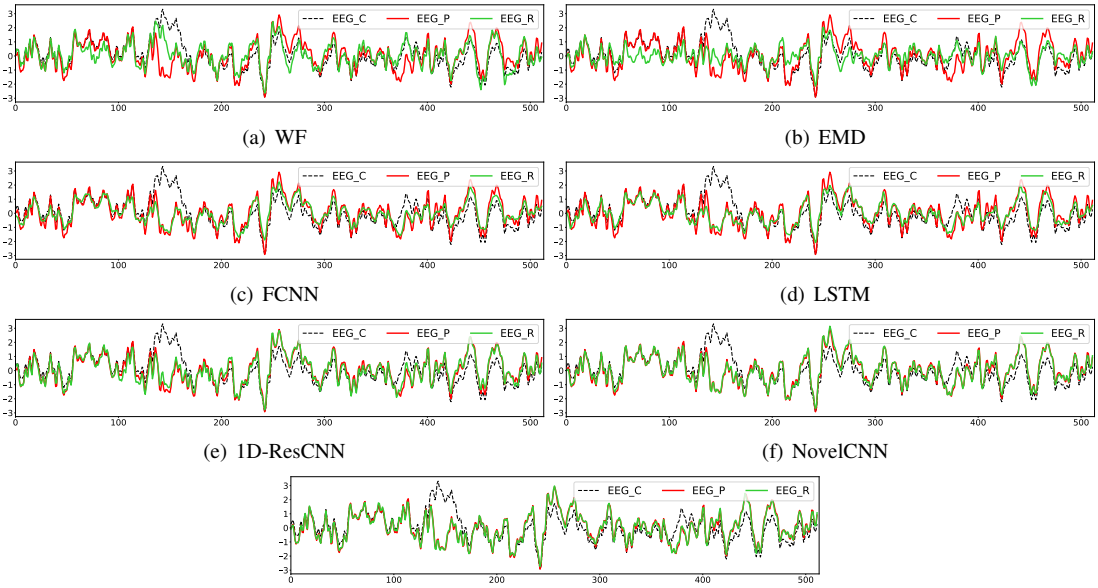

(a) WF (b) EMD

(c) FCNN (d) LSTM

(e) 1D-ResCNN (f) NovelCNN

(g) DuoCL

Fig. 3: Example of experimental result waveform for eliminating EOG artifacts.

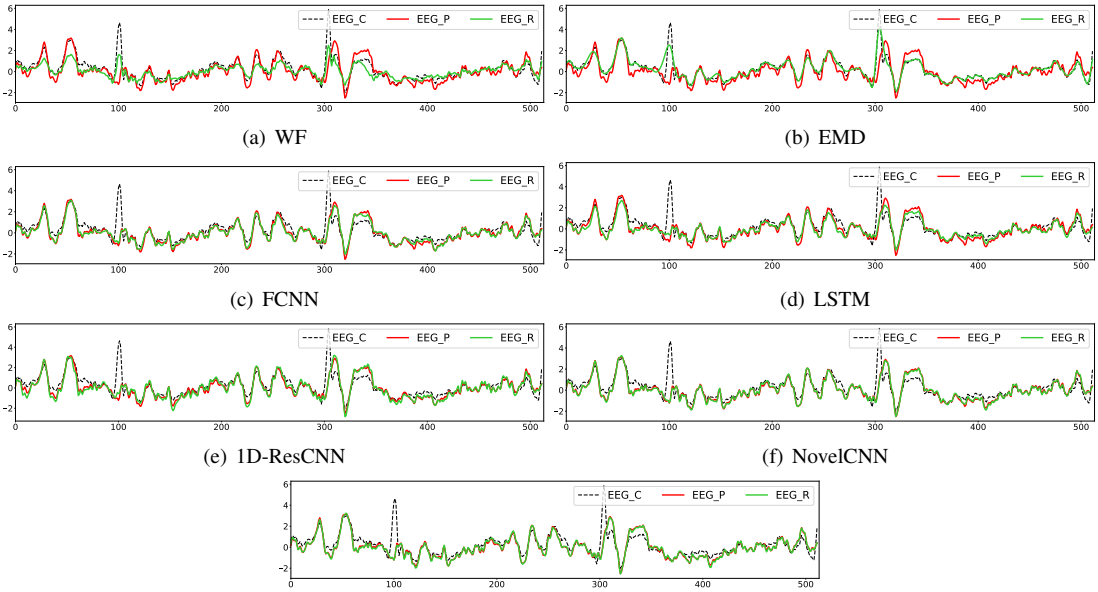

(a) WF (b) EMD

(c) FCNN (d) LSTM

(e) 1D-ResCNN (f) NovelCNN

(g) DuoCL

Fig. 4: Example of experimental result waveform for eliminating ECG artifacts.

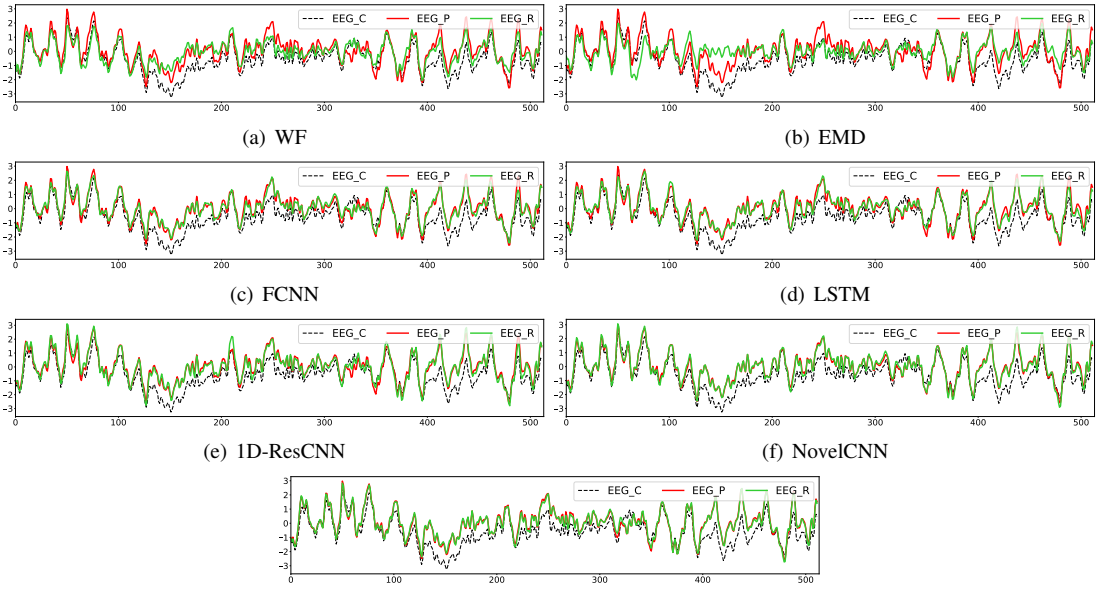

(a) WF (b) EMD

(c) FCNN (d) LSTM

(e) 1D-ResCNN (f) NovelCNN

(g) DuoCL

Fig. 5: Example of experimental result waveform for eliminating EM artifacts.

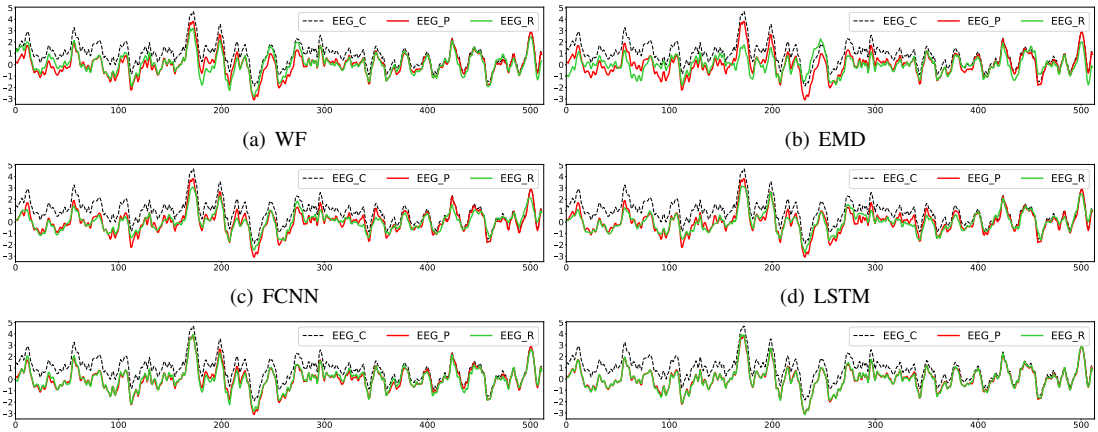

(a) WF (b) EMD

(c) FCNN (d) LSTM

(e) 1D-ResCNN (f) NovelCNN

Fig. 6: Example of experimental result waveform for eliminating BW artifacts.

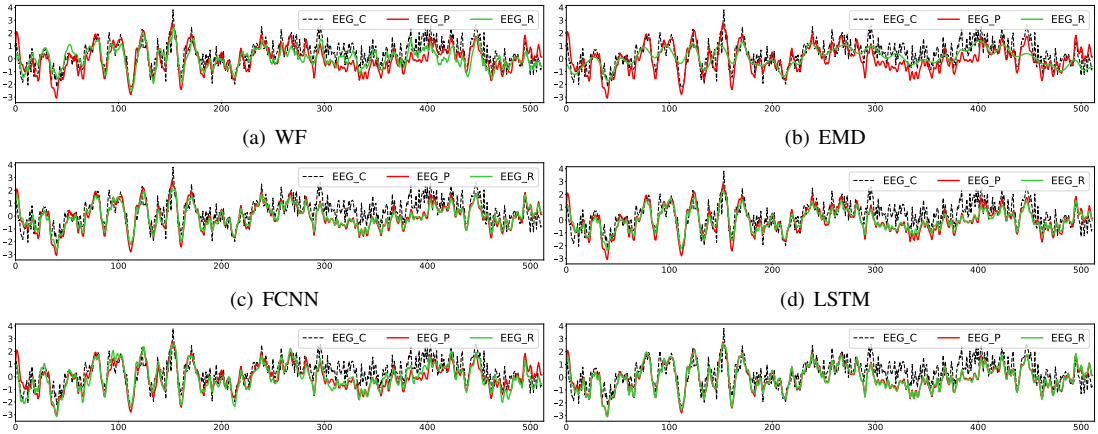

(a) WF (b) EMD

(c) FCNN (d) LSTM

(e) 1D-ResCNN (f) NovelCNN

Fig. 7: Example of experimental result waveform for eliminating BW+EMG artifacts.

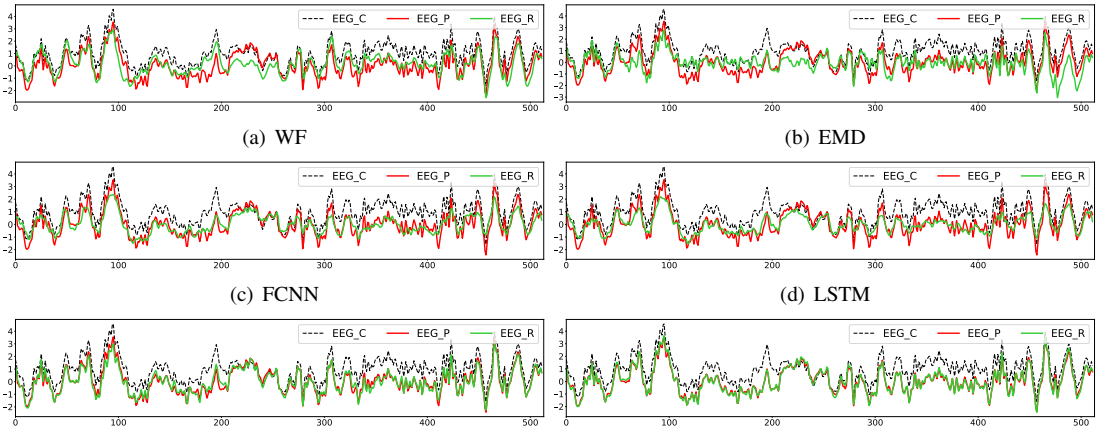

(a) WF (b) EMD

(c) FCNN (d) LSTM

(e) 1D-ResCNN (f) NovelCNN

Fig. 8: Example of experimental result waveform for eliminating EMG+EOG+BW artifacts.

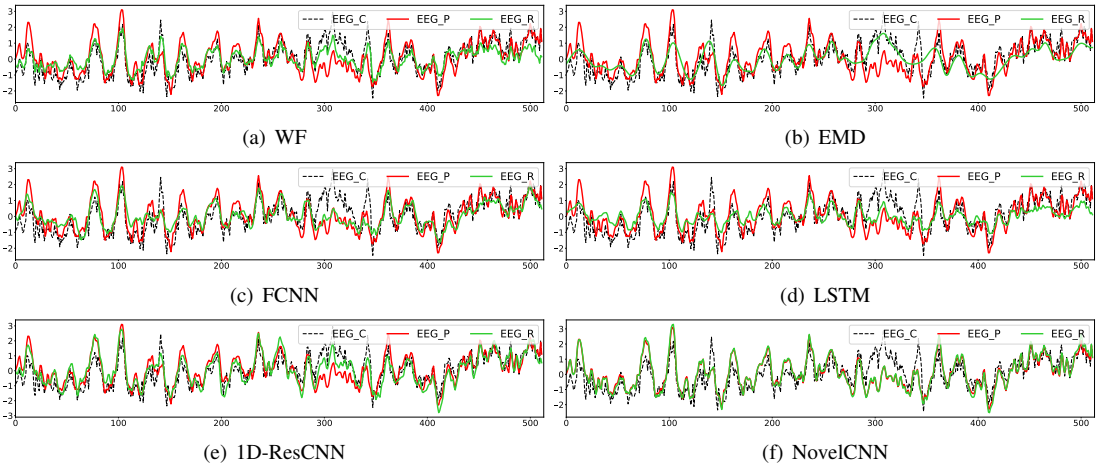

(a) WF (b) EMD

(c) FCNN (d) LSTM

(e) 1D-ResCNN (f) NovelCNN

Fig. 9: Example of experimental result waveform for eliminating EMG+EOG+BW+ECG artifacts.

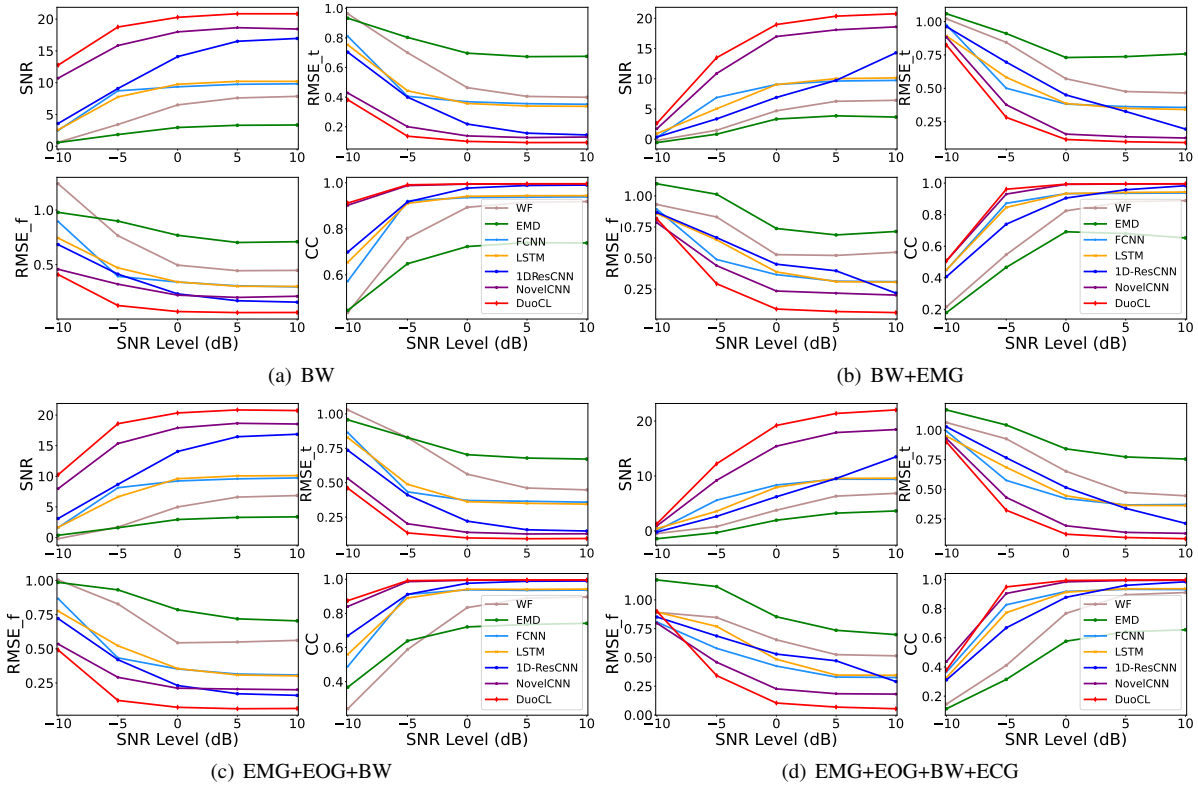

(a) BW (b) BW+EMG

(c) EMG+EOG+BW (d) EMG+EOG+BW+ECG

Fig. 10: Experimental results at different SNR levels after unknown & hybrid artifact removal.

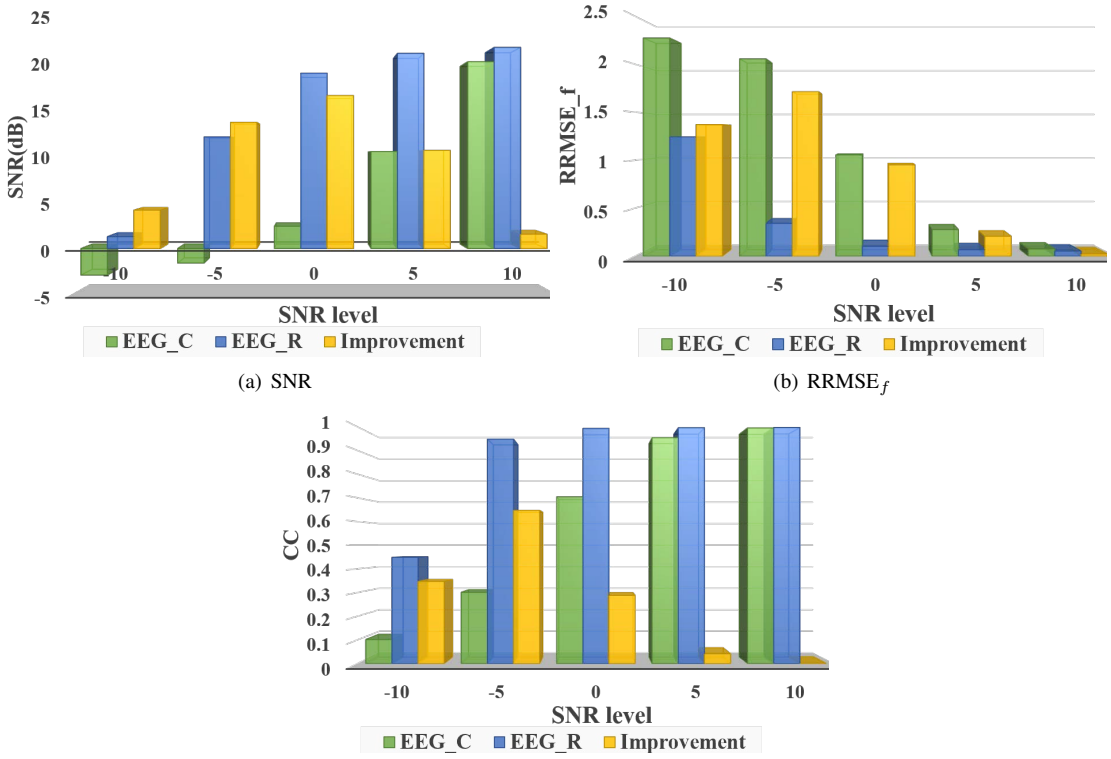

(a) SNR (b) RRMSE$_f$

(c) CC

Fig. 11: Results and degree of improvements of DuoCL before and after removal of hybrid artifacts (EMG+EOG+BW+ECG) at different contamination levels